# Effects of the Nozzle Configuration with and without an Internal Guide Vane on the Efficiency in Cross-Flow Small Hydro Turbines

Fredys Romero-Menco [1], Juan Pineda-Aguirre [1], Laura Velásquez [1], Ainhoa Rubio-Clemente [1,2] and Edwin Chica [1,*]

1    Grupo de Energía Alternativa, Facultad de Ingeniería, Universidad de Antioquia, Calle 70 No 52-21, Medellín 050010, Colombia; dejesus.romero@udea.edu.co (F.R.-M.); jdavid.pineda@udea.edu.co (J.P.-A.); lisabel.velasquez@udea.edu.co (L.V.); ainhoa.rubioc@udea.edu.co (A.R.-C.)
2    Escuela Ambiental, Facultad de Ingeniería, Universidad de Antioquia, Calle 70 No. 52-21, Medellín 050010, Colombia
*    Correspondence: edwin.chica@udea.edu.co; Tel.: +57-6042195550

**Abstract:** In this work, an experimental analysis of the performance of a cross-flow turbine, commonly referred to as a Michell–Banki turbine (MBT), is carried out for small-scale hydropower production in rural areas located in developing countries to support their social and economic development activities. The study investigates how the efficiency of the MBT is influenced by the presence or absence of a nozzle, along with variations in the internal guide vane (GV) and its angle. The runner had 26 blades that were arranged symmetrically in the periphery between two circular plates. The designed MBT had the ability to generate a maximum of 100 W of power at a water flow rate and a head of 0.009 $m^3$/s and 0.6311 m, respectively. The experimental tests were carried out using a hydraulic bench. The turbine efficiency without the inner GV was found to be higher than that of the turbine with the inner GV; i.e., it was found that the utilization of the GV did not enhance the efficiency of the MBT due to the occurrence of a choking effect. A maximum hydraulic efficiency of 85% was achieved in the turbine without an inner GV in comparison with the efficiency achieved (77%) with this device and an optimum opening angle of the GV of 24° (75% of opening). In this regard, the GV design should be carefully carried out to improve the MBT efficiency. Additionally, the effect of the GV shape on the MBT performance should be experimentally investigated to obtain a more general judgment regarding the role of this device.

**Keywords:** cross-flow turbine; Michell–Banki turbine; hydropower; small hydro turbine; nozzle; turbine efficiency; opening percentage

## 1. Introduction

Electricity generation from hydroelectric power sources is still deserving of the first position concerning the use of renewable sources of energy, as it is widely distributed worldwide [1–3]. Indeed, 16% of the global electricity is produced from hydropower. In 2021, this technology had an installed power capacity of 1330 GW [4]. Harnessing this energy source holds promise for making substantial contributions to the reduction in greenhouse gas (GHG) emissions, the security of the energy supply and the mitigation of global warming compared to conventional oil power plants [5–8]. Additionally, and in order to foster the balance among other intermittent renewable sources on the grid, hydropower plants are highlighted as hydroelectricity is a very reliable energy. Compared with other renewable energy sources, hydropower has a broad distribution, a good stability and a high utilization efficiency [4].

In a hydropower plant, the potential energy of water moving from higher to lower elevation is harnessed to produce electricity proportionally to the product of water discharge

and pressure head [5]. Initially, the potential energy is transformed into mechanical energy via the rotation of a turbine. Afterward, the mechanical energy is converted into electrical energy using an electric generator powered by the turbine [4].

There are two types of hydropower plant: (i) Impoundment facilities, i.e., large hydropower systems that take profit of the river water stored in a dam. In this system, the water stored flows through a turbine, spinning it and activating a generator to produce electricity. (ii) Run-of-river power plants. This setup comprises a diversion structure directing a segment of a river through a channel, eliminating the necessity for a dam [6]. Several types of hydraulic turbines can be named: impulse turbines (e.g., Turgo, Michell–Banki, Pelton) and reaction turbines (e.g., Deriaz, Kaplan, Francis), gravity turbines (e.g., water wheels, Archimedes screws), which primarily harness kinetic energy, water pressure and gravitational force, respectively [4]. Reaction and impulse turbines can be used in large or small hydropower plants. The key factors to contemplate during the design and selection of a hydropower turbine for a particular project are the volume or rate of the water flow and the elevation difference, known as the head, at the location [9].

Hydropower plants have several advantages and good potential; however, the development of this technology can be difficult, especially when large projects are undertaken, as they are often extremely disruptive. Furthermore, when they are not sensitively developed, a range of environmental problems can be produced. It is important to note that large projects require that large land areas are flooded, resulting in several social and environmental impacts, such as the destruction of natural fauna and flora habitats, and the displacement of wildlife and people. In contrast, small hydro schemes, if properly designed, are easily integrated into local ecosystems [6,10,11].

North America and Europe are recognized worldwide due to their production of electricity from hydropower. Nevertheless, Latin America, Asia and Africa have attracted the attention of the global community due to their potential for the implementation of new hydro plants. Therefore, small hydroelectric power plants are an alternative means of generating electricity in rural areas of developing nations without access to the national power grid [12]. In this regard, the challenges related to access to electricity are expected to be overcome [11].

In order to foster rural electrification, at present, technologies involving photovoltaic and small-scale hydropower systems and wind and hydrokinetic turbines merit further attention in non-developed countries [12]. Most rural electrification programs have been focused on generating electricity using small hydropower system in regions that have perennial rivers and mountainous topographies [11]. However, the equipment used in these systems, especially the turbine, is often not optimized for the conditions of the installation site. To ensure an effective energy supply solution, it is necessary to employ small turbines that offer a balance between cost-effectiveness and efficiency [5].

The cross-flow turbine, also known as the Michell–Banki turbine (MBT), presents an attractive choice for small-scale hydropower production due to its straightforward design and relatively low initial investment (due to its simplicity and inexpensive manufacture, allowing it to be easily produced by local facilities). Additionally, this kind of technology has a relatively high efficiency [13]. This turbine has a modest efficiency, between 70 and 85% over a wider range of flow [14–16]. While the maximum peak efficiency achieved by the cross-flow turbine may be less than that of traditional hydraulic turbine types, such as Kaplan, Pelton, or Francis turbines, it is crucial to significantly enhance its efficiency to ensure the competitiveness of this technology. This can only be achieved by numerical and experimental research focused on the turbine's operation and the determination of the parameters and phenomena affecting its performance. According to the literature reports, the MBT's efficiency depends on different combinations of several physical and geometric factors concerning the turbine. Among the physical factors, the flow rate, the pressure on the shaft and the total head are named. The geometric parameters encompass factors such as the geometry of the nozzle and characteristics of the runner, which include the diameter ratio ($D_2/D_1$), the outer diameter of the runner ($D_1$), the number of blades, the

shaft diameter (d), blade thickness, runner side wall thickness, orientation of the nozzle guide vane (GV), the angle of admission arc of the nozzle, blade curvature, blade exit angle for the initial stage and the angle between the relative water jet velocity entering the turbine and the outer periphery of the turbine [17–21]. Some of the studies conducted on MBT are presented as follows.

Pereira and Borges conducted an experiment where the nozzle flow in a cross-flow turbine was analyzed. Two nozzle types, one with an inner GV and another without the GV, were examined. The referred authors found that the nozzle with the GV had the best characteristics. The nozzle without an inner GV led water to poorly enter the runner, leading to a lower efficiency [22]. In turn, Kokubu et al. noted that incorporating a GV within the nozzle may enhance the turbine's efficiency. Nonetheless, they observed that the GV does not ensure a consistent head at the turbine inlet [23].

Numerical studies also were carried out. Chen and co-workers investigated the cross-flow turbine's performance using the GV by means of CFD software. Their research revealed that the cross-flow turbine with an inner GV positioned at 20° exhibited favorable operational characteristics. Operating the turbine at this GV angle resulted in a higher efficiency [24]. Acharya et al. found, from a numerical point of view, that incorporating the GV improves the efficiency of the cross-flow turbine, increasing it from 63.67% (in the base model) to 67.26%. Additionally, Acharya et al. varied the GV and demonstrated that by varying the GV angle in 7°, the efficiency increased from 67.26% to 73.09% [16]. Dragomirescu numerically investigated the variation in the GV angle from 0° to 20° and concluded that the GV allowed could maintain the absolute velocity angle if the GV angle was closer to 16°. It is worth noting that varying the absolute velocity led to a higher turbine efficiency [25].

Adhikari and Wood [20], in turn, concluded that a flow control that differs from the inner GV in the turbine is required to maintain a high efficiency. For example, to redesign the nozzle shape, as proposed for the referred authors, a system consisting of a sliding circular segment for the inflow regulation can be used [26]. This segment rotated on the periphery of the runner to adjust the nozzle inlet area, allowing for control of the turbine so that efficiency values above 86% were obtained.

Saini et al. conducted a numerical investigation into the effects of the GV placement on the turbine efficiency and the flow-field distributions [27]. They examined the performance of the cross-flow turbine model with and without the GV, varying the operating conditions. Their observations indicated reduced turbulence and vortex formations, which were attributed to the optimized GV placement within the runner. This facilitated a defined pathway for the smooth entry of water into the second stage of the blade.

In contemporary cross-flow turbine design advancements, the integration of nozzles, the inner GV, or valves is a common practice, aimed at regulating flow and enhancing the turbine's power generation capacity. However, the inclusion of the GV may compromise the quality of the inlet flow by dividing it into two jets and generating a non-uniform entry flow angle, consequently diminishing the turbine's efficiency. Therefore, some researchers advocate for the development of smaller-scale models devoid of the GV [1,19,28–30]. Despite these considerations, the influence of nozzles in smaller cross-flow turbine models has received limited attention, and consensus within the scientific community regarding the advantages associated with incorporating a GV inside the nozzle to improve the turbine efficiency is lacking. In this regard, experimentally verifying the effect of the GV positioned inside the nozzle is required.

Therefore, the main aim of this study is to experimentally examine the impact of the nozzle with and without an inner GV, as well as the impact of the GV angle on the MBT efficiency, in order to discern whether the GV in the nozzle could improve the turbine's efficiency.

## 2. Materials and Methods

### 2.1. Components of the MBT

The MBT consists of two essential components: a runner (rotating component) and a nozzle (stationary component) [27]. The runner is fabricated using two parallel discs, joined together by multiple curved blades [17,28]. Some designs include a GV in the nozzle, as illustrated in Figure 1. The GV controls the water flow rate entering the turbine. During partial load operation, flow separation from the leading edge of the GV may cause the flow under the GV to deviate from the optimal direction.
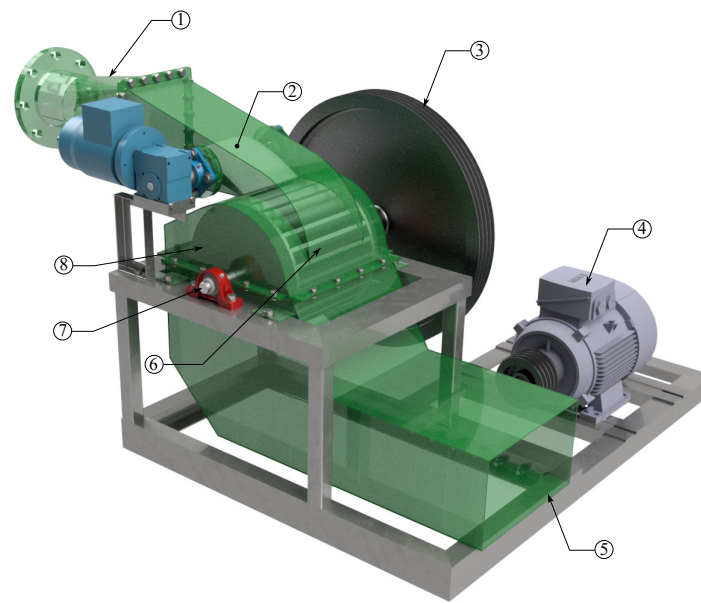


**Figure 1.** Component of a cross-flow turbine: 1—Nozzle; 2—Inner guide vane (GV); 3—Transmission (belts and pulley drives); 4—Generator; 5—Draft tube; 6—Runner; 7—Shaft; 8—Casing.

Anthony Michell invented the cross-flow turbine in 1904. Donat Banki significantly improved this turbine circa 1918 [13]. The MBT qualifies as a cross-flow turbine due to the interaction between the water jet and the blades, occurring as the blades approach the nozzle (first stage), followed by the flow of the water jet from the outlet to the inlet of the same blades once they reach the opposite side (second stage) [31]. As a result, the turbine blades experience the impact of the water flow twice. Due to its operational flexibility and ease of manufacturing, the MBT is an adaptable hydropower technology suitable for deployment across various hydraulic settings and geographic locations [32]. In fact, the MBT can be operated in areas with flow rates and heads below <10 m$^3$/s and 200 m, respectively [33].

The hydraulic efficiency ($\eta$) of this turbine is defined as the ratio of the power output ($P_{out}$) to the power input ($P_{in}$), as outlined in Equation (1).

$$\eta = \frac{P_{out}}{P_{in}} = \frac{T\omega}{\rho g Q H} \tag{1}$$

where the shaft torque, the runner angular velocity, the water density and the gravity acceleration are expressed by T (N m), $\omega$ (rad/s), $\rho$ (1000 kg/m$^3$) and g (9.81 m/s$^2$), respectively. Additionally, H and Q are the net head (m) and the flow rate (m$^3$/s), respectively [32]. H can be measured through the well-known Bernoulli equation (Equation (2)).

$$H = \frac{P_{pre}}{\rho g} + \frac{V^2}{2g} + h \tag{2}$$

where $P_{pre}$ is the pressure gauge (N/m$^2$) at the inlet point, V represents the water velocity at the turbine inlet (measued in m/s), while h denotes the disparity in the height of the pressure transducer and the center of the MBT runner (measured in m).

### 2.2. Experimental Setup and Design Parameters

Experimental tests were conducted in the hydraulic laboratory located within the Department of Mechanical Engineering at Universidad de Antioquia (Colombia). The setup comprised a water pumping system and a testing platform featuring a model of an MBT, developed by the Alternative Energy Research Group at the aforementioned institution. The turbine model was developed according to the standardized design established by the Latin America Energy Organization (OLAE) [34]. The cross-flow turbine components are illustrated in Figure 2. In the figure, the runner blades, the turbine disc, the shaft nozzle, the GV and the casing can be observed. The runner had an inner and an outer diameter of 103.02 mm and 156.107 mm, respectively. Additionally, the runner contained 26 blades. The inner blade angle ($\alpha$) and outer blade angle ($\beta$) were set at 30° and 90°, respectively. The dimensions of the nozzle, runner, and runner chamber were 177.3 mm, 253.2 mm, and 290 mm in width, respectively. The nozzle was oriented in a horizontal position, and was manufactured from a stainless-steel sheet. The GV was designed for 0° of inclination with respect to the horizontal line. This device was adjusted for several flow conditions. The GV angle was assessed over a range from 32° to 0°, representing the transition from fully closed to fully open states for the turbine, respectively. The GV opening interval was defined as a percentage for convenience, using 0% and 100% to represent totally closed and opened, respectively. This angle is represented by $\gamma$, as shown in Figure 3b.
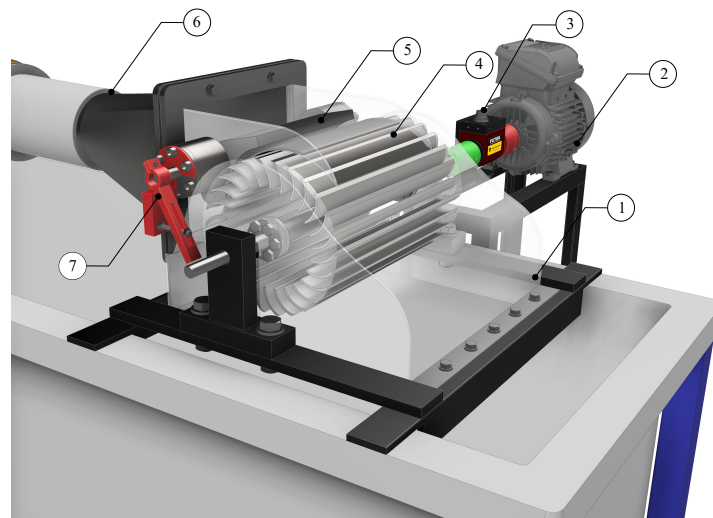


**Figure 2.** Experimental model of a cross-flow turbine: 1—casing; 2—brake motor; 3—torque sensor; 4—runner; 5—nozzle; 6—transition; 7—opening control system.

The runner, constructed in a straightforward manner, resembles a squirrel cage and is composed of two circular discs made of transparent acrylic sheet connected by curved horizontal blades and a shaft. Moreover, the runner blades were crafted by cutting stainless-steel sheets and subsequently bending them to achieve the necessary blade profile. The circular discs were of 5 mm thickness and were cut and trim for 26 blades using the Computer Numerical Control (CNC) Machining process. The blades were fit into slots contained within the discs and glued using an epoxy resin. The central shaft was also manufactured of stainless steel and had a thickness of 12 mm diameter. It was screwed to the discs using two flanges. The geometric factors are listed in Table 1. Finally, the casing was made of acrylic and steel.

The turbine performance was measured in terms of the maximum efficiency for 12 experimental configurations that are detailed in Table 2. The efficiency of the turbine

($\eta$) was calculated using Equation (1). The performance test established the best efficiency point, for which the general turbine performance was determined by varying the runner speed, the head and the flow.
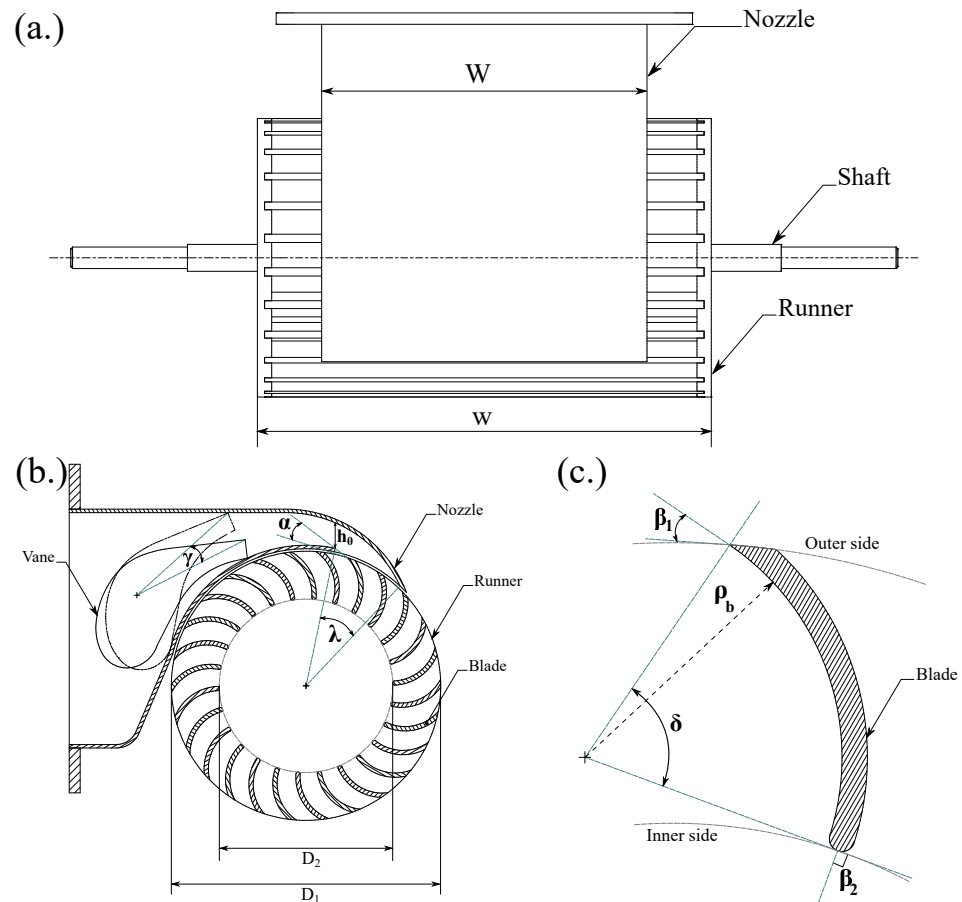


**Figure 3.** Schematic representation of design parameters for an experimental MBT: (**a.**) Plan view of the nozzle and runner; (**b.**) cross-section of the turbine with GV in fully open and fulyl closed positions; (**c.**) blade parameter details.

**Table 1.** Design parameters of the tested experimental MBT model.

| MBT Design Factor | Value |
|---|---|
| Inner diameter ($D_2$), (mm) | 103.02 |
| Outer diameter ($D_1$), (mm) | 156.107 |
| Runner width ($w$), (mm) | 253.2 |
| Angle of attack ($\alpha$), (°) | 16.102 |
| Inner blade angle ($\beta_2$),(°) | 30 |
| Outer blade angle ($\beta_1$), (°) | 90 |
| Blade radius ($\rho_b$), (mm) | 25.88 |
| Number of blades (Z) | 26 |
| Nozzle throat ($h_o$), (mm) | 6.1 |
| Nozzle width ($W$), (mm) | 177.3 |
| Nozzle entry arc ($\lambda$), (°) | 17 |

**Table 2.** Experimental configurations.

| Configuration | Guide Vane (GV) | Flow Rate (m³/s) |
|---|---|---|
| MBT with GV (25% opening) | Yes | 0.0050 |
| MBT with GV (25% opening) | Yes | 0.0038 |
| MBT with GV (25% opening) | Yes | 0.0025 |
| MBT with GV (50% opening) | Yes | 0.0050 |
| MBT with GV (50% opening) | Yes | 0.0038 |
| MBT with GV (50% opening) | Yes | 0.0025 |
| MBT with GV (75% opening) | Yes | 0.0050 |
| MBT with GV (75% opening) | Yes | 0.0038 |
| MBT with GV (75% opening) | Yes | 0.0025 |
| MBT without GV | No | 0.0050 |
| MBT without GV | No | 0.0038 |
| MBT without GV | No | 0.0025 |

The experiments were conducted utilizing the hydraulic bench depicted in Figure 4. This setup comprises interconnected pipes connecting an upper and lower reservoir, facilitating the circulation of water. Functioning as a recirculating water system, it possesses a natural static head of 30 m. Additionally, the hydraulic bench is furnished with flow meters, a control system, pressure transducers, electrical generators, valves, and a data acquisition system.
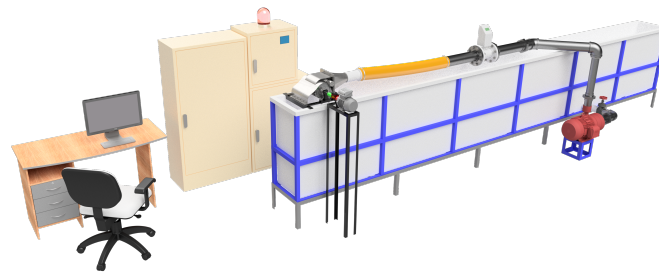


**Figure 4.** Schematic design of the hydraulic test bench for experimental tests.

Water from the lower reservoir is recirculated to the upper one by a centrifugal pump of 11 kW, a head of 90 m and a flow rate of 50 m³/h. The reservoir section measures 0.35 m in width, 0.5 m in height and 5 m in length, resulting in a maximum capacity of 2 m³. The centrifugal pump set supplies the water from the sump tank to the turbine through a control valve and a human–machine interface (HMI) facilitating communication between a desktop computer and the control board, in which frequency variators (Siemens 440 6SE6440 of 15 HP $\pm$ 0.1 Hz) (Siemens AG, Munich, Germany) are installed. In the HMI, the flow rate setpoint is introduced and a signal is transferred to the variators, which control the rotation speed of the pumps delivering the established flow rate. With this control system, different operational regimes can be obtained.

T and $\omega$ at the shaft outlet were measured using a rotary torque sensor with an encoder (Futek-Model TRS605) (Futek, Irvine, CA, USA) to determine the turbine power. To achieve this, the sensor was tightly integrated with the turbine shaft alongside a drive brake (as shown in Figure 2). Real-time data collection was facilitated using an intelligent digital handheld display (IHH500 Pro) (Futek, Irvine, CA, USA) connected to the sensor. During each experiment, the torque sensor shaft was attached to an electric motor of 1 HP (Siemens, 1LA7 073-2YA60) (Siemens AG, Munich, Germany), which worked as a brake, using the reverse current braking technique. This consists of energizing the motor in the inverse rotating direction to the turbine, generating a reverse torque and reducing the turbine $\omega$. Thus, in this method, the motor works as an electric power generator that is braked for the power demand. The torque brake was adjusted depending on the turbine $\omega$. The current flowing to the motor was regulated for a frequency variator selected according

to the motor capacity (Siemens 440 6SE6440 of 1.0 HP $\pm$ 0.1 Hz) (Siemens AG, Munich, Germany), allowing for the frequency to be controlled starting at 1 Hz. This frequency was regulated using a constant slope braking ramp of 0.1 Hz each 10 s until reaching the total brake of the turbine. Thereby, $\omega$ and T were measured in each load. An electromagnetic flow meter (Siemens Sitrans MAGFLO 6000 $\pm$ 0.2%) (Siemens AG, Munich, Germany), installed in the supply pipeline was used for the flow rate measurements. Finally, the head was estimated using the pressure in the supply pipeline. For this purpose, a dial manometer (USH 0-30 kPa $\pm$ 1 kPa) (USH, Hilchenbach, Germany), which was installed perpendicular to the pipeline and at a distance equivalent to five rotor diameters upstream of the turbine, was used to guarantee that the pressure measures were reliable.

Using the measured values of head, water flow rate, $\omega$ and T recorded by the sensor, the experimental efficiency ($\eta$) of the turbine was computed using Equation (1).

## 3. Results and Discussion

The experiments were conducted using three values of flow, including 2.5 L/s (0.0025 m$^3$/s), 3.8 L/s (0.0038 m$^3$/s) and 5.0 L/s (0.005 m$^3$/s), with the purpose of evaluating the turbine's performance and discerning its behavior at different flow rates.

Figure 5 represents the turbine performance as a function of $\omega$ for a flow rate of 0.0025 m$^3$/s. The experimental data are represented by points, and a fit curve was drawn using these points. For the turbine with the GV, the highest $\eta$ was reached for an opening of 75% at 110 RPM, resulting in an efficiency value close to 77%. Meanwhile, the lowest $\eta$ was obtained for an opening of 25% at 105 RPM, where the value of $\eta$ increased to 50%. On the other hand, the turbine $\eta$ without the GV was 85% at $\sim$102 RPM, which means that an improvement of 10% was obtained compared with the turbine $\eta$ at an opening of 75%. Additionally, the operating range of the turbine without GV was wider compared with that of the turbine with the GV installed. Some researchers argue that the use of GV results in the flow being split into two parts. As a result, there is a decrease in efficiency (as noted by [32]) due to deceleration and alterations in flow trajectory, resulting in an uneven velocity profile at the runner inlet and deviation from the ideal direction.
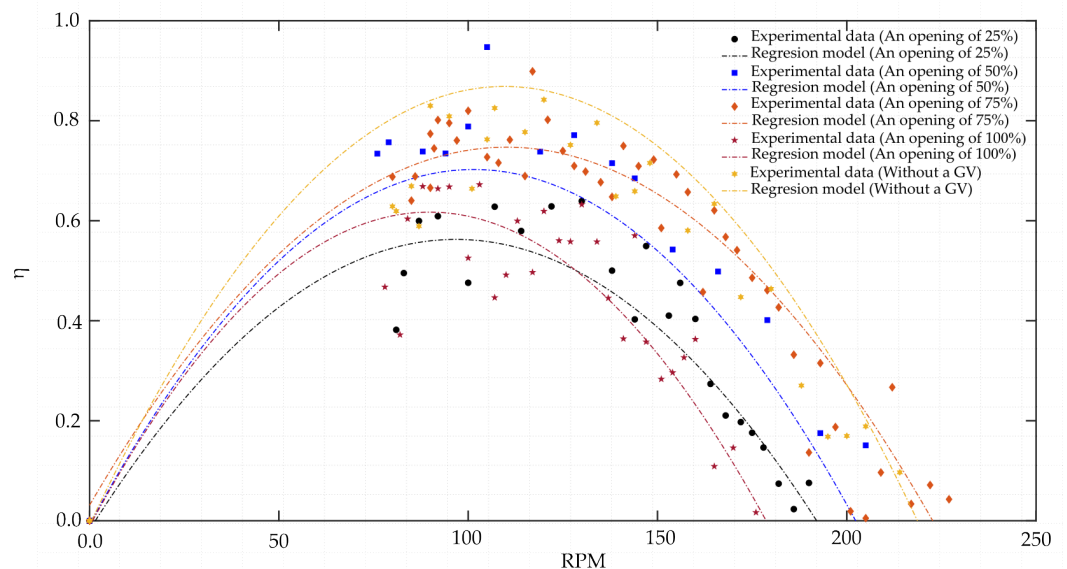


**Figure 5.** Experimental results for the MBT model at a flow rate of 0.0025 m$^3$/s.

The value of $\eta$ was diminished when employing the inner guide vane (GV), attributed to heightened friction and choke losses within the runner. It can be speculated that a segment of the flow rate deviates from the optimal pathway towards the runner. Therefore, the GV should be carefully designed for the operating conditions of the MBT. In this regard, new experimental studies must be carried out to discern the GV geometry effect on the

turbine efficiency, and correctly conclude whether the blade has a significant effect on the MBT efficiency.

Figure 6 corresponds to the results of the turbine experiments for a 0.0038 m$^3$/s flow rate. Like the results obtained for a flow rate of 0.0025 m$^3$/s for the turbine with the GV installed, the best behavior was observed up to an opening of 75%. In this case, a maximum $\eta$ of 68%, close to 140 RPM, was achieved. The poorest performance observed was for the opening of 25%, in which $\eta$ was equal to 43% at 130 RPM. For the turbine without the GV, $\eta$ was near 72% at 132 RPM, which is 4% higher than the better value reached when the GV is used. In this case, the difference between the turbine efficiency with and without the GV is smaller than the results obtained previously for 0.0025 m$^3$/s of the flow rate. Likewise, in general terms, the maximum efficiency values are lower compared with those reached at the mentioned flow rate. Nevertheless, the operation rotational speed range is higher for the 0.0038 m$^3$/s flow rate compared with the results obtained for the flow rate of 0.0025 m$^3$/s. Finally, for the turbine without the GV, the operational speed range was wider compared with the range in the presence of the GV.



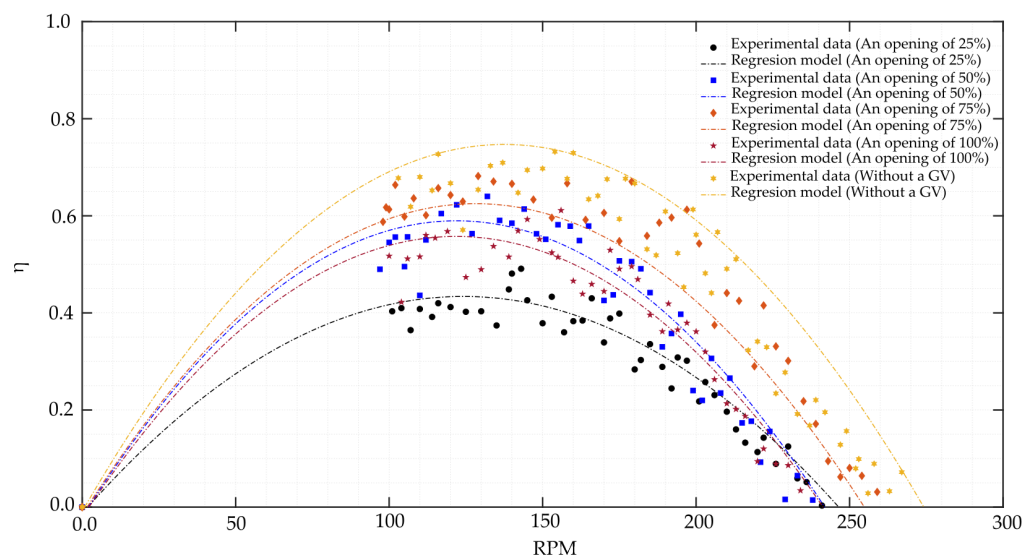**Figure 6.** Experimental results for the MBT model at a flow rate of 0.0038 m$^3$/s.

Concerning the flow rate of 0.005 m$^3$/s, the efficiency results are shown in Figure 7. In this case, similarly to the previous findings, the turbine with the GV and an opening of 75% exhibited the highest $\eta$, reaching, on this occasion, a value of 63% at 165 RPM. The lowest $\eta$ was observed for the turbine with an opening of 25%, close to 155 RPM, dropping close to 35%. For the turbine without GV, a $\eta$ of 65% was reached at 165 RPM, as presented for the turbine with the GV. For this flow rate, the difference between the turbine with and without the GV was only 2%. Moreover, the difference in the rotational operation range for the turbine exhibiting better behavior with and without GV is smaller compared with the results for the turbine with the previously analyzed flow rate.

Finally, in Figure 8, the efficiency for the turbine without GV for different flow rates is compared. As can be seen, as the flow rate increases, the maximum efficiency points were reached at higher $\omega$ values. On other hand, the highest efficiency drop of 15.29% occurred between the flow rates of 0.0025 m$^3$/s and 0.0038 m$^3$/s, going from 85% to 72%, whereas between the flow rates of 0.0038 m$^3$/s and 0.005 m$^3$/s, $\eta$ reduction was 7%. This phenomenon can explain the increase in the turbulence intensity at the nozzle. According to the studies reported in the literature, when the fluid flows through the nozzle to reach the maximum energy interchange condition, it is necessary that the fluid behave as ordered and the stream tubes are oriented so that the turbulence at the nozzle does not affect the MBT performance [35].
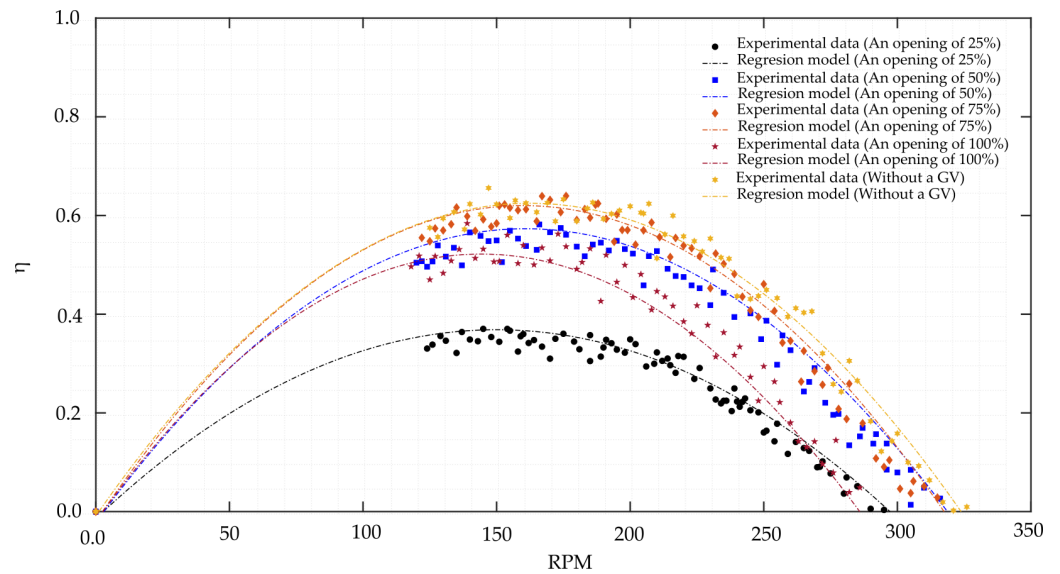
**Figure 7.** Experimental results for the MBT model at a flow rate of 0.005 m$^3$/s.
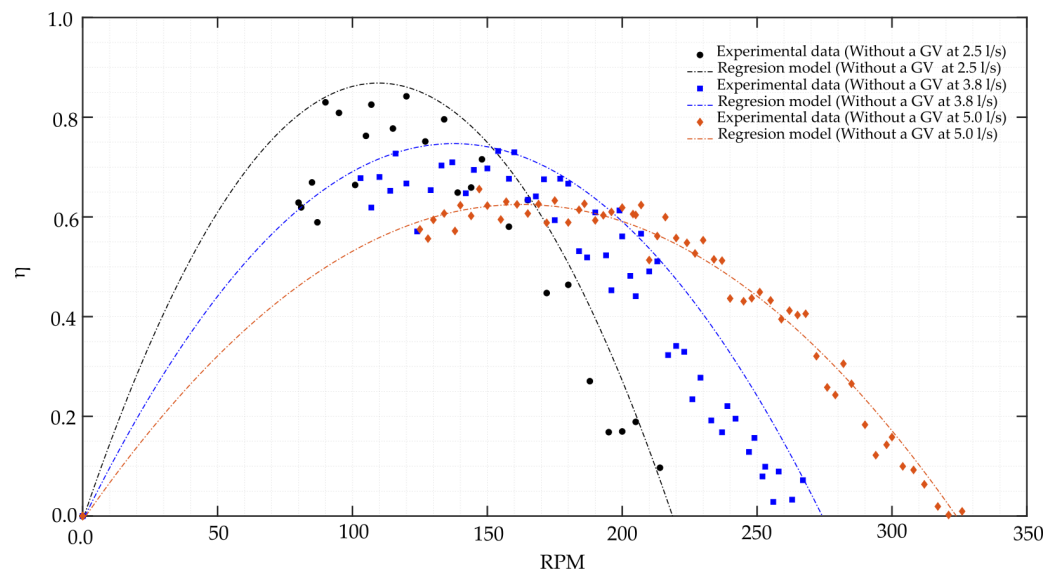


**Figure 8.** Experimental results for the MBT model without GV at different flow rates.

Table 3 shows the hydraulic efficiency for the tested experimental configurations. This table presents the efficiency values corresponding to each of the configurations evaluated during the experiments. Hydraulic efficiency is a critical indicator of the turbine performance and provides insights into the ability to effectively convert hydraulic energy into mechanical energy. Analyzing these values allows for a better understanding of how various variables, such as the presence of an internal GV in the nozzle or the GV opening percentage, affect the turbine's overall performance. It can be observed that the highest efficiency of 85% was achieved for a flow rate of 0.0025 m$^3$/s without a GV, while the lowest efficiency of 35% was attained for the turbine configuration with an inner GV, a flow rate of 0.005 m$^3$/s and a GV opening percentage of 25%.

**Table 3.** Results of experimental configurations.

| Configuration | Guide Vane (GV) | Flow Rate (m³/s) | Hydraulic Efficiency ($\eta$) |
|---|---|---|---|
| MBT with GV (25% opening) | Yes | 0.0050 | 35% (at 155 RPM) |
| MBT with GV (25% opening) | Yes | 0.0038 | 43% (at 130 RPM) |
| MBT with GV (25% opening) | Yes | 0.0025 | 50% (at 105 RPM) |
| MBT with GV (50% opening) | Yes | 0.0050 | 59% (at 175 RPM) |
| MBT with GV (50% opening) | Yes | 0.0038 | 55% (at 125 RPM) |
| MBT with GV (50% opening) | Yes | 0.0025 | 69 % (at 99 RPM) |
| MBT with GV (75% opening) | Yes | 0.0050 | 63% (at 165 RPM) |
| MBT with GV (75% opening) | Yes | 0.0038 | 68% (at 140 RPM) |
| MBT with GV (75% opening) | Yes | 0.0025 | 77% (at 110 RPM) |
| MBT without GV | No | 0.0050 | 65% (at 165 RPM) |
| MBT without GV | No | 0.0038 | 72% (at 132 RPM) |
| MBT without GV | No | 0.0025 | 85% (at 102 RPM) |

On the other hand, the improvement in the maximum point of $\eta$ between the turbine with and without the GV can be produced with decreased pressure due to the presence of this device. In the designs proposed by Sammartano et al. and Sinagra and co-workers [21,30,35], the turbine nozzle was developed to be operated without GV. Instead, these authors proposed the use of a slider plate with a semi-circular shape that slides around the periphery of the rotor, arguing that, in this case, the device acts on the entry angle amplitude without causing a fluid deceleration and preserving the energy available within the fluid. This is clearer when comparing an opening of 25% with other opening values. At this opening point, in the GV at the trailing edge, a boundary layer separation zone is formed, leading to a highly turbulent wake just before the fluid enters to the runner. Additionally, due to the position and the shape of the GV, this device becomes a wall, causing energy dissipation and leading to a pressure drop in the fluid, which means less energy is transferred to the rotor. As the opening increases, the efficiency is also increased. Nevertheless, contrary to the expected behaviour for the MBT model used, the lowest pressure drop occurs at an opening of 75%. At an opening of 100%, the pressure drop increases because of the GV shape.

## 4. Conclusions

The efficiency of the Michel–Banki turbine (MBT) was found to be lower compared to conventional turbines that are commonly used. To determine the optimal configuration for the MBT, numerical and experimental studies have been reported in the literature. These investigations have focused on various factors, such as the runner diameter, the blade quantity, the blade shape, the nozzle design, the admission arc and the incorporation of an inner guide vane (GV). Nevertheless, there is conflicting evidence regarding the effectiveness of the GV within the nozzle, since some studies supported its use while others did not. Consequently, the impact of the GV on the turbine performance remains poorly understood. Therefore, this study aimed to experimentally validate the effect of the inner GV on the MBT performance. Additionally, the research analyzed the turbine performance at various GV opening percentages across three different flow rates.

According to the results obtained, the best performance of the turbine with the GV was exhibited at an opening of 75%, which was equivalent to 24° in the turbine experimental model that was used. In average, the value of $\eta$ reached at this point was 69%. On the other hand, the lowest $\eta$ for different flow rates was reached at an opening of 25%. At this opening point, during the experiments, a boundary layer separation in the GV trailing edge occurred, which could explain the poor efficiency obtained under these operating conditions (an average value of 43%).

Concerning the turbine without the GV, $\eta$ values were higher in comparison with the turbine with this device. However, these efficiency values drop for inflow rates of 0.0038 m³/s and 0.005 m³/s. For the turbine model used, the $\eta$ value without the GV

fluctuated between 65% and 85%. This decrease was likely due to the nozzle shape, which was not designed to operate without the GV, or because the GV should be carefully designed for the MBT operating conditions. In addition, when the flow rate was increased, the turbulence intensity in the nozzle became strong, acting as an energy dissipation source before being transferred to the MBT rotor.

Finally, as the GV used in this research negatively affected the turbine performance, other mechanism of flow control can be estimated and analyzed with the objective of designing a turbine that operates at high efficiency values for different flow rates. Further studies are needed concerning the GV shape in order to better understand the effect of this device on the MBT efficiency.

**Author Contributions:** Writing—original draft preparation, F.R.-M.; methodology, F.R.-M., E.C. and A.R.-C.; formal analysis, J.P.-A., L.V., A.R.-C. and E.C.; experimental setup, F.R.-M., J.P.-A., L.V., A.R.-C. and E.C.; writing—review and editing, A.R.-C. and E.C.; funding acquisition, A.R.-C. and E.C.; project administration, A.R.-C. and E.C.; supervision, E.C. All authors have read and agreed to the published version of the manuscript.

**Data Availability Statement:** Data are contained within the article.

**Conflicts of Interest:** The authors declare no conflicts of interest.

## References

1. Woldemariam, E.T.; Lemu, H.G.; Wang, G.G. CFD-driven valve shape optimization for performance improvement of a micro cross-flow turbine. *Energies* **2018**, *11*, 248. [CrossRef]
2. Yuksek, O.; Komurcu, M.I.; Yuksel, I.; Kaygusuz, K. The role of hydropower in meeting Turkey's electric energy demand. *Energy Policy* **2006**, *34*, 3093–3103. [CrossRef]
3. Frey, G.W.; Linke, D.M. Hydropower as a renewable and sustainable energy resource meeting global energy challenges in a reasonable way. *Energy Policy* **2002**, *30*, 1261–1265. [CrossRef]
4. Bilgili, M.; Bilirgen, H.; Ozbek, A.; Ekinci, F.; Demirdelen, T. The role of hydropower installations for sustainable energy development in Turkey and the world. *Renew. Energy* **2018**, *126*, 755–764. [CrossRef]
5. Berga, L. The role of hydropower in climate change mitigation and adaptation: A review. *Engineering* **2016**, *2*, 313–318. [CrossRef]
6. Sharma, S.; Waldman, J.; Afshari, S.; Fekete, B. Status, trends and significance of American hydropower in the changing energy landscape. *Renew. Sustain. Energy Rev.* **2019**, *101*, 112–122. [CrossRef]
7. Bousquet, C.; Samora, I.; Manso, P.; Rossi, L.; Heller, P.; Schleiss, A.J. Assessment of hydropower potential in wastewater systems and application to Switzerland. *Renew. Energy* **2017**, *113*, 64–73. [CrossRef]
8. Carvajal, P.E.; Li, F.G.; Soria, R.; Cronin, J.; Anandarajah, G.; Mulugetta, Y. Large hydropower, decarbonisation and climate change uncertainty: Modelling power sector pathways for Ecuador. *Energy Strat. Rev.* **2019**, *23*, 86–99. [CrossRef]
9. Okot, D.K. Review of small hydropower technology. *Renew. Sustain. Energy Rev.* **2013**, *26*, 515–520. [CrossRef]
10. Bakken, T.H.; Sundt, H.; Ruud, A.; Harby, A. Development of small versus large hydropower in Norway–comparison of environmental impacts. *Energy Procedia* **2012**, *20*, 185–199. [CrossRef]
11. Hecht, J.S.; Lacombe, G.; Arias, M.E.; Dang, T.D.; Piman, T. Hydropower dams of the Mekong River basin: A review of their hydrological impacts. *J. Hydrol.* **2019**, *568*, 285–300. [CrossRef]
12. Ioannidou, C.; O'Hanley, J.R. Eco-friendly location of small hydropower. *Eur. J. Oper. Res.* **2018**, *264*, 907–918. [CrossRef]
13. Leguizamón, S.; Avellan, F. Computational parametric analysis of the design of cross-flow turbines under constraints. *Renew. Energy* **2020**, *159*, 300–311. [CrossRef]
14. Olgun, H. Investigation of the performance of a cross-flow turbine. *Int. J. Energy Res.* **1998**, *22*, 953–964. [CrossRef]
15. Olgun, H. Effect of interior guide tubes in cross-flow turbine runner on turbine performance. *Int. J. Energy Res.* **2000**, *24*, 953–964. [CrossRef]
16. Acharya, N.; Kim, C.G.; Thapa, B.; Lee, Y.H. Numerical analysis and performance enhancement of a cross-flow hydro turbine. *Renew. Energy* **2015**, *80*, 819–826. [CrossRef]
17. Oliy, G.B.; Ramayya, A.V. Design and computational fluid dynamic simulation study of high efficiency cross flow hydro-power turbine. *Int. J. Sci. Technol. Soc.* **2017**, *5*, 120–125. [CrossRef]
18. Nasir, B.A. Design of high efficiency cross-flow turbine for hydro-power plant. *Int. J. Eng. Adv. Technol.* **2013**, *2*, 308–311.

19. Choi, Y.D.; Lim, J.I.; Kim, Y.T.; Lee, Y.H. Performance and internal flow characteristics of a cross-flow hydro turbine by the shapes of nozzle and runner blade. *J. Fluid Sci. Technol.* **2008**, *3*, 398–409. [CrossRef]

20. Adhikari, R.; Wood, D. A new nozzle design methodology for high efficiency crossflow hydro turbines. *Energy Sustain. Dev.* **2017**, *41*, 139–148. [CrossRef]

21. Sammartano, V.; Morreale, G.; Sinagra, M.; Tucciarelli, T. Numerical and experimental investigation of a cross-flow water turbine. *J. Hydraul. Res.* **2016**, *54*, 321–331. [CrossRef]

22. Pereira, N.C.; Borges, J. Study of the nozzle flow in a cross-flow turbine. *Int. J. Mech. Sci.* **1996**, *38*, 283–302. [CrossRef]

23. Kokubu, K.; Son, S.W.; Kanemoto, T.; Choi, Y.D. Internal flow analysis on a micro cross-flow type hydro turbine at very low specific speed range. In Proceedings of the 11th Asian International Conference on Fluid Machinery, Chennai, India, 21–23 November 2011.

24. Chen, Z.; Choi, Y.D. Performance and internal flow characteristics of a cross-flow turbine by guide vane angle. *IOP Conf. Ser. Mater. Sci. Eng.* **2013** , *52*, 052031. [CrossRef]

25. Dragomirescu, A. Numerical investigation of the flow in a modified Bánki turbine with nozzle foreseen with guide vanes. In Proceedings of the 2016 International Conference and Exposition on Electrical and Power Engineering (EPE), Iasi, Romania, 20–22 October 2016; IEEE: Piscataway, NJ, USA, 2016; pp. 874–879.

26. Adhikari, R.; Wood, D. Computational analysis of part-load flow control for crossflow hydro-turbines. *Energy Sustain. Dev.* **2018**, *45*, 38–45. [CrossRef]

27. Saini, G.; Saini, R.; Singal, S. Numerical investigations on performance improvement of cross flow hydro turbine having guide vane mechanism. *Energy Sources Part Recover. Util. Environ. Eff.* **2022**, *44*, 771–795. [CrossRef]

28. Adhikari, R.; Wood, D. The design of high efficiency crossflow hydro turbines: A review and extension. *Energies* **2018**, *11*, 267. [CrossRef]

29. Haurissa, J.; Wahyudi, S.; Irawan, Y.S.; Soenoko, R. The cross flow turbine behavior towards the turbine rotation quality, efficiency, and generated power. *J. Appl. Sci. Res.* **2012**, *8*, 448–453.

30. Sinagra, M.; Sammartano, V.; Aricò, C.; Collura, A.; Tucciarelli, T. Cross-Flow turbine design for variable operating conditions. *Procedia Eng.* **2014**, *70*, 1539–1548. [CrossRef]

31. Verma, V.; Gaba, V.K.; Bhowmick, S. An experimental investigation of the performance of cross-flow hydro turbines. *Energy Procedia* **2017**, *141*, 630–634. [CrossRef]

32. Quaranta, E.; Perrier, J.P.; Revelli, R. Optimal design process of crossflow Banki turbines: Literature review and novel expeditious equations. *Ocean Eng.* **2022**, *257*, 111582. [CrossRef]

33. Khaniya, B.; Priyantha, H.G.; Baduge, N.; Azamathulla, H.M.; Rathnayake, U. Impact of climate variability on hydropower generation: A case study from Sri Lanka. *ISH J. Hydraul. Eng.* **2020**, *26*, 301–309. [CrossRef]

34. Bazo, C.A.H. *Manual de Diseño, Estandarización y Fabricación de Equipos para Pequeñas Centrales Hidroeléctricas*; Olade: San Carlos, Ecuador, 1985.

35. Sammartano, V.; Aricò, C.; Carravetta, A.; Fecarotta, O.; Tucciarelli, T. Banki-Michell optimal design by computational fluid dynamics testing and hydrodynamic analysis. *Energies* **2013**, *6*, 2362–2385. [CrossRef]